Development 139, 397-410 (2012) doi:10.1242/dev.065581

Sox2 and Mitf cross-regulatory interactions consolidate progenitor and melanocyte lineages in the cranial neural crest

Igor Adameyko[1], Francois Lallemend[1], Alessandro Furlan[1], Nikolay Zinin[2], Sergi Aranda[1], Satish Srinivas Kitambi[1], Albert Blanchart[1], Rebecca Favaro[3], Silvia Nicolis[3], Moritz Lübke[1], Thomas Müller[4], Carmen Birchmeier[4], Ueli Suter[5], Ismail Zaitoun[6], Yoshiko Takahashi[7] and Patrik Ernfors[1,*]

SUMMARY

The cellular origin and molecular mechanisms regulating pigmentation of head and neck are largely unknown. Melanocyte specification is controlled by the transcriptional activity of Mitf, but no general logic has emerged to explain how Mitf and progenitor transcriptional activities consolidate melanocyte and progenitor cell fates. We show that cranial melanocytes arise from at least two different cellular sources: initially from nerve-associated Schwann cell precursors (SCPs) and later from a cellular source that is independent of nerves. Unlike the midbrain-hindbrain cluster from which melanoblasts arise independently of nerves, a large center of melanocytes in and around cranial nerves IX-X is derived from SCPs, as shown by genetic cell-lineage tracing and analysis of *ErbB3*-null mutant mice. Conditional gain- and loss-of-function experiments show genetically that cell fates in the neural crest involve both the SRY transcription factor Sox2 and Mitf, which consolidate an SCP progenitor or melanocyte fate by cross-regulatory interactions. A gradual downregulation of *Sox2* in progenitors during development permits the differentiation of both neural crest- and SCP-derived progenitors into melanocytes, and an initial small pool of nerve-associated melanoblasts expands in number and disperses under the control of endothelin receptor B (Ednrb) and Wnt5a signaling.

KEY WORDS: Schwann cell precursor, Cell fate, Melanocyte, Multipotency, Neural crest, Stem cells, Mouse

INTRODUCTION

Most melanocytes in vertebrates originate from the neural crest (NC). The neural crest cells (NCCs) delaminate from the neural tube, migrate through the periphery (Dorris, 1938; Dorris, 1939; DuShane, 1935; Rawles, 1947; Twitty, 1936) and differentiate into various cell types. The fate of delaminating NCCs is correlated with their temporal emergence (Krispin et al., 2010). Early cells migrate ventrally providing peripheral glia, sympathetic and sensory neurons (Marmigere and Ernfors, 2007), whereas later cells adopt a melanocyte fate. Melanocytes migrate in a dorsolateral pathway and are instructed by Wnt1 and Wnt3a emanating from the dorsal neural tube at the developmental period when Bmp4 expression in the neural tube decreases (Jin et al., 2001). Recent results described an alternative origin and migratory pathway of melanocyte progenitor cells in the trunk: melanocytes arise from Schwann cell precursors (SCPs) located in nerves projecting throughout the embryo (Adameyko et al., 2009; Budi et al., 2011). SCPs are believed to be a transient cell population formed during development from NCCs of the ventral migratory pathway in the trunk that can differentiate into Schwann cells. Within the nerves, neuregulin 1 inserted into the axonal membrane of motor and sensory neurons promotes a glial and inhibits a melanocyte fate, whereas insulin-like growth factor (IGF) and platelet-derived growth factor (PDGF) produced by maturing Schwann cells promote a melanocyte fate of SCPs in the nerves (Adameyko and Lallemend, 2010; Adameyko et al., 2009; Ernfors, 2010). However, the origin of melanocytes in the head region has remained unclear. In the chick, metencephalic NC (rhombomeres 1 and 2 of the neural crest) is a major source of NC-derived trigeminal ganglion neurons (Baker et al., 1997; Noden, 1975), whereas mesencephalic NCCs contribute to skin melanocytes of the head (Baker et al., 1997). In mouse, the use of reporter genes suggested the existence of several clusters of cranial melanocytes, which subsequently migrate to cover the head and neck. Analysis of mice carrying expression of *lacZ* from the melanin-synthesizing enzyme dopachrome tautomerase (Dct; *Dct-lacZ* mice) promoter suggested that cranial melanoblasts migrate rostrally from a cluster of cells in the cervical region (Mackenzie et al., 1997; Wilkie et al., 2002), whereas expression studies of pigment cell-specific transmembrane protein encoded by *Pmel17* (*Pmel* – Mouse Genome Informatics) suggest a mesencephalic origin with melanoblasts migrating laterally along two primary pathways (Baxter and Pavan, 2003).

All melanocytes are specified by the basic helix-loop-helix-zipper transcription factor Mitf, which is an activator of many of the genes required for melanogenesis. Another transcription factor, the HMG-type DNA-binding factor Sox2, which is expressed in the neural epithelium, acts as a transcriptional activator and functionally inhibits neuronal and glial differentiation (Bylund et al., 2003; Le et al., 2005). Sox2 is also expressed in the NC, but its function during

[1]Unit of Molecular Neurobiology, Department of Medical Biochemistry and Biophysics, Karolinska Institute, 17177 Stockholm, Sweden. [2]Department of Microbiology, Tumor and Cell Biology, Karolinska Institute, 17177 Stockholm, Sweden. [3]Department of Biotechnology and Biosciences, University of Milano-Bicocca, Piazza della Scienza 2, 20126 Milano, Italy. [4]Max-Delbrück-Centrum for Molecular Medicine, Robert-Rössle-Strasse 10, 13125 Berlin, Germany. [5]Institute of Cell Biology, Department of Biology, ETH Zürich, CH-8093 Zürich, Switzerland. [6]Department of Neuroscience, University of Wisconsin School of Medicine and Public Health, 1300 University Avenue, Madison, WI 53706, USA. [7]Graduate School of Biological Sciences, Nara Institute of Science and Technology, 8916-5, Takayama, Ikoma, Nara, 630-0192, Japan.

*Author for correspondence: (patrik.ernfors@ki.se)

Accepted 10 November 2011

melanocyte development has not been addressed (Aquino et al., 2006; Wakamatsu et al., 2004; Wakamatsu et al., 2000). To determine the origin and the transcriptional mechanisms underlying melanoblast specification and the factors expanding specified melanocytes in the neck and head, we used a variety of preparations. We found that cranial melanocytes emerge in discrete foci and are of distinct cellular origins; some arise from SCPs whereas others might be derived directly from NCCs. The development of melanocytes from both NC and SCP origin involves repressive cross-regulatory interactions between *Sox2* and *Mitf*, and an initial small number of melanocytes associated with nerves expand by signaling via endothelin 3 (Edn3) and Wnt5a. These results might provide a general logic for development of SCPs into myelinating Schwann cells and melanocytes in which Sox2 maintains an SCP progenitor state and its cross-regulatory interactions with either Krox20 (Egr2 – Mouse Genome Informatics) or Mitf result in a commitment to myelinating Schwann cells or melanocytes, respectively (schematically illustrated in Fig. 6H).

MATERIALS AND METHODS

Mouse strains and genetic tracing

All animal work was conducted according to Swedish national and international guidelines. The generation and characterization of *PLP-CreERT2*, *ErbB3*$^{-/-}$ and *Sox2*$^{fl/fl}$ mice have been previously described (Favaro et al., 2009; Leone et al., 2003; Maro et al., 2004). *Wnt1Cre* mice (Danielian et al., 1998) were ordered from The Jackson Laboratory (stock number 003829). *Wnt5a* knockout mice (Yamaguchi et al., 1999) were ordered from The Jackson Laboratory (stock number 004758). Conditional *Ednrb* knockout mice have been described previously (Druckenbrod et al., 2008; Druckenbrod and Epstein, 2009).

PLP-CreERT2 mice were combined with a reporter allele *Rosa26YFP* for genetic tracing (Srinivas et al., 2001). During the genetic tracing experiment with *PLP-CreERT2/Rosa26YFP* mice, the pregnant females were injected with 1 mg per animal of tamoxifen (TM) intraperitoneally at embryonic day (E) 9.5.

Plasmids, siRNAs, cell lines and reagents

In ovo electroporations of plasmids and siRNAs were carried out as previously described (Marmigere et al., 2006). The set of plasmids with doxycyclin-inducible promoters was a gift of Dr Yoshiko Takahashi (Watanabe et al., 2007).

The open reading frames of *Sox2*, *Sox2-ENR* and *Sox2-VP16* were a gift of Dr Jonas Muhr (Bylund et al., 2003). STEALTH siRNAs were designed and ordered against chick *Mitf* using Invitrogen online tool BLOCK-iT RNAi Designer (https://rnaidesigner.invitrogen.com/rnaiexpress/index.jsp): siRNA1, 5′-CAAACCAGCCCGGUGAUCAUGUCAU-3′; siRNA2, 5′-GAUGGAUGAUGUGAUUGAUGACAUA-3′; scrambled control, 5′-GCAGACAGAGGGAGUUUGUUACGCA-3′.

The two tet-on plasmids (one with GFP and another with the place for the gene of interest) were fused together into one large vector using restriction enzyme *Pvu*II and ligation. After this manipulation, we produced one vector carrying two identical doxycyclin-inducible promoters controlling expression of GFP and the gene of our interest (*Sox2* or *Mitf*).

The vector with *Renilla* luciferase reporter under the control of proximal Mitf-m promoter was a gift of Prof. Carol Erickson and Prof. Aaron Thomas (Thomas and Erickson, 2009). The open reading frame of *Sox10* was received from Prof. Peter Farlie (McKeown et al., 2005). The mouse melanoma cell line B16-F10 was ordered from ATCC (ATCC-CRL-6475). Transfection was carried out as previously described (Thomas and Erickson, 2009). The Dual-Luciferase Assay Reporter System (Promega) was used for assessing the activity of the Mitf-m promoter.

Sectioning and immunohistochemistry

Embryos were fixed in 4% paraformaldehyde (PFA) in PBS, cryoprotected and sectioned at a thickness of 14-μm. The TSA Plus Cyanine System from PerkinElmer (NEL744B001KT) was used to perform the tyramide signal amplification (TSA) reaction as described by the manufacturer. The optimal dilution of the Mitf antibody for TSA was 1:50,000. Images were taken using a Carl Zeiss LSM5 Exciter confocal microscope and analyzed with Image J.

For immunohistochemistry, we used the following antibodies: rabbit anti-Mitf that detects all Mitf isoforms (gift from Makoto Mochii) (Mochii et al., 1998), goat anti-Mitf (R&D Systems), rabbit anti C-kit (Cell Signaling Technology) mouse anti-MEBL1 (gift from Yoshio Wakamatsu) (Kitamura et al., 1992; Kushimoto et al., 2001), mouse anti-Neurofilament (2H3, Developmental Studies Hybridoma Bank), mouse anti-βIII tubulin (Promega), mouse anti-Cre (USBiologicals), guinea pig anti-Foxd3 and rabbit anti-BFabp [generated by Thomas Muller, Max Delbrück Center for Molecular Medicine (MDC) in Berlin-Buch, Germany], guinea pig anti-Sox10 [gift from Michael Wegner, Friedrich-Alexander-Universität Erlangen-Nürnberg (FAU), Germany], and rabbit anti-Sox2 [gift from Thomas Edlund, Umeå Centre for Molecular Medicine (UCMM), Sweden]. Cryostat sections were processed for immunostaining as previously described (Marmigere et al., 2006) with fluorophore-conjugated secondary antibodies (Alexa, Molecular Probes).

Whole-mount immunohistochemistry of mouse embryos, 3D imaging, visualization and analysis

Whole-mount fluorescent immunostaining of mouse embryos was performed as described previously (Huber et al., 2005) with some minor modifications to improve the specific signal with antibodies against nuclear antigens. These modifications of the original protocol were as follows: after 6 hours in 4% PFA embryos were washed three times in PBST (phosphate-buffered saline with 0.1% Tween 20; 10 minutes each wash) and then eventually transferred into 100% methanol through a standard series of increasing methanol concentrations (25%, 50%, 75%). After 24 hours of incubation in 100% methanol at 4°C, embryos were transferred directly into bleaching solution (1 part of 30% hydrogen peroxide to 2 parts of 100% methanol) for another 24 hours (4°C), then washed three times with 100% methanol (10 minutes each at room temperature), postfixed with Dent's Fixative (1 part dimethyl sulfoxide to 4 parts methanol) overnight (4°C) and stored in this solution at –20°C. Subsequently, embryos were transferred into PBST through a standard series of decreasing methanol concentrations and incubated with primary antibodies. For optimum staining, embryos were incubated for 4-6 days at room temperature with 2H3, Bfabp, Mitf and Foxd3 antibodies at 1:1000 or for 4 days at 4°C with the Sox10 antibody at 1:1000.

Three-dimensional (3D) imaging of whole-mount mouse embryos stained with different antibodies was performed using a Carl Zeiss LSM5 Exciter confocal microscope and Carl Zeiss Cell Observer SD spinning disc microscope. Confocal stacks were produced containing 50 to 200 optical slices. Bitplane IMARIS software was used for 3D visualization and analysis of confocal stacks. To avoid high levels of noise, stacks were rendered in 3D and non-specific fluorescent background (which appeared as numerous small diameter ultra-bright speckles in both the red and infrared channels used to record Mitf, Foxd3 and Sox10 nuclear staining) was removed. The non-specific speckles were much smaller in diameter (1-2 μm) than cell nuclei (8-15 μm), allowing them to be removed using the volume filtering option in IMARIS without affecting specific nuclear staining (supplementary material Fig. S18). Quantification of the cells inside rendered 3D volumes was carried out with IMARIS by counting generated isosurfaces within the requested volume range and outlined 3D area. For graphs shown in Fig. 6O-Q, the quantified 3D area corresponded to the field of view of Zeiss 20× objective with 0.8 numerical aperture in *xy* dimensions, i.e. 636.8 μm. Depth of scanning, or the *z*-axis dimension, was adjusted individually for every sample in order to reach the neural tube midline starting from embryonic epidermis (on average 200-300 μm).

Chromatin immunoprecipitation (ChIP)

ChIP assays were performed using a commercial kit (Millipore) following the manufacturer's instructions. Mouse embryonic stem (mES) cells were grown for 48 hours as described previously (Andang et al., 2008). Chromatin was immunoprecipitated with 10 μg of either rabbit Sox2 antibody (Millipore) or a normal rabbit IgG (Invitrogene) as control.

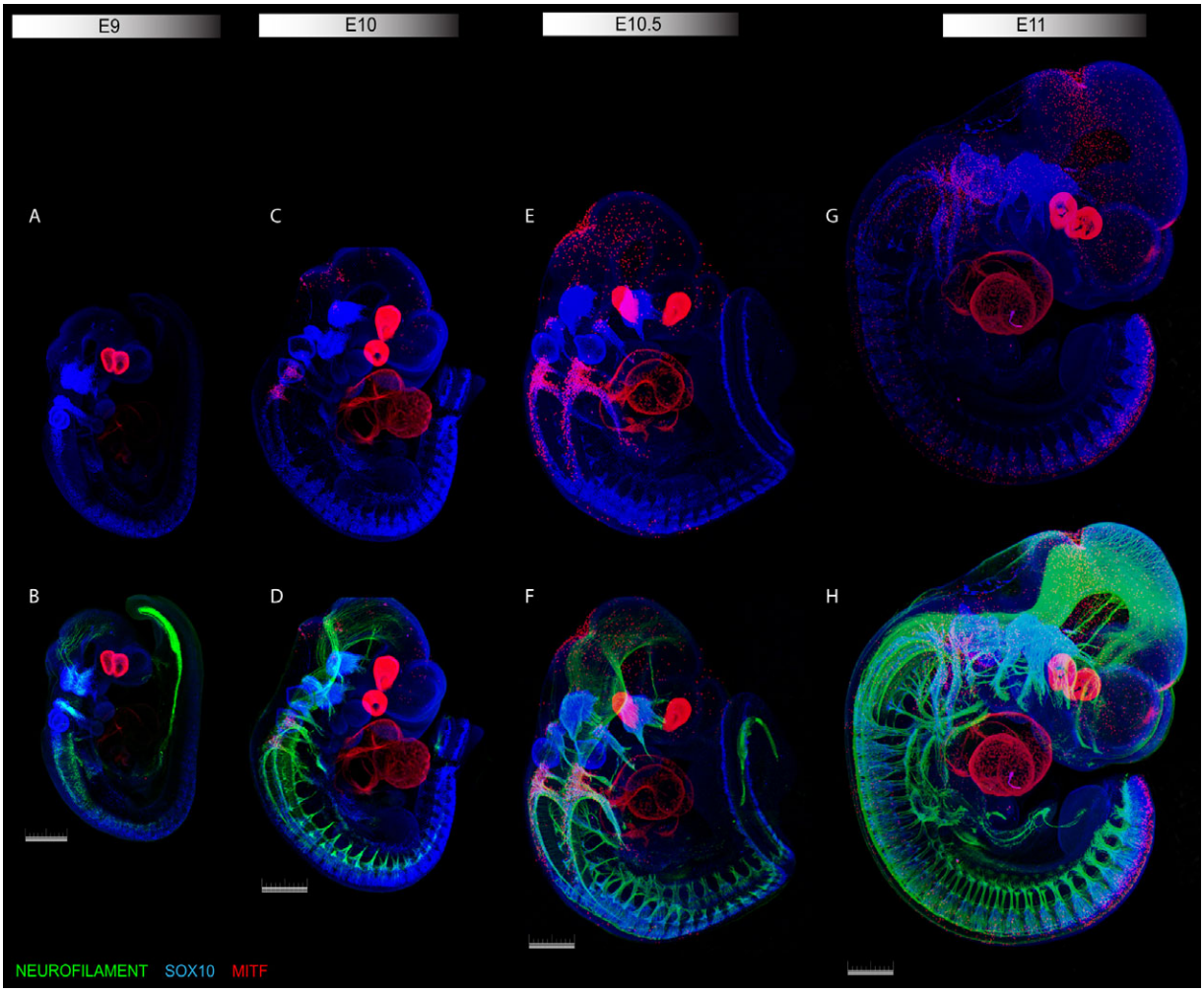

Fig. 1. Overview of melanocyte development during mouse embryonic development visualized using 3D projection images. Melanocyte development in relation to nervous tissues visualized by Sox10 (blue), Mitf (red) and NF (green) immunohistochemical staining. A, C, E and G show Sox10 and Mitf channels, and B, D, F and H show all three channels. (**A**,**B**) E9 embryo. Note nascent cranial ganglia V, VII-VIII, IX-X without any apparent Sox10$^+$ NCC migration. (**C-H**) Note the emergence of Mitf$^+$ cells in IX-X and hindbrain-midbrain clusters at E10 (C,D), their expansion at E10.5 (E,F) and dispersal at E11.0 (G,H). Scale bars: 500 μm.

The primers designed for PCR amplification were: pMitf-F1, 5′-GGCAATGTCCCCTCTGAAGAGGGC-3′; pMitf-R1, 5′-GCTCACTGT-CAGATCAAGGCC-3′; pMitf-F2, 5′-GTGAGCTTGACTTTGAT-AGCTC-3′; pMitf-R2, 5′-CAGCTTATAATAACCTAAGC-3′.

Endothelin-3 and Dct in situ hybridization

For riboprobe synthesis, 645 nucleotides of mouse *Edn3* and 1000 nucleotides of *Dct* from open reading frames (GenBank NM_007903 and NM_010024.3, respectively) were synthesized and cloned in pBSKS vector by Epoch Life Science. In situ hybridization on E9.5-11 mouse embryos was carried out as described previously (Adameyko et al., 2005).

RESULTS

Developmental emergence and molecular characteristics of melanoblasts during mouse development

In order to define the emergence of NC- and SCP-derived melanoblasts in the developing mouse embryo, we used whole-mount immunohistochemistry followed by 3D visualization. We used an anti-Mitf antibody to identify melanoblasts, an anti-Sox10 antibody to visualize NCCs and SCPs, and an anti-neurofilament 165 kDa (2H3) antibody to visualize peripheral and central neurons and their projections. By applying 3D imaging, the timing and distribution of developing melanocytes were studied from E9 to E11 (10-20 embryos/stage; Fig. 1; supplementary material Fig. S1).

Sox10 is not only expressed in NCCs but is also a critical transcription factor for melanocyte development during which, together with Pax3, it drives Mitf expression (Bondurand et al., 2000; Potterf et al., 2000; Watanabe et al., 1998). Hence, melanocytes develop from Sox10$^+$ NCCs, and Sox10 expression persists in such cells after the onset of Mitf expression. At E9, numerous Sox10$^+$ NCCs were observed close to the dorsal neural tube at cranial, thoracic and lumbar levels of the embryo, consistent with their migration and contribution to cranial and trunk structures (Fig. 1A,B; supplementary material Movie 1). Scattered Sox10$^+$ cells were observed in the rostral part of the head, coalescing dorsal root ganglia (DRG) and cranial ganglia (V, VII-VIII, IX-X) and in ventral parts of the embryo at the forelimb level (developing gut) (Fig. 1A,B, Fig. 2A-H; supplementary material Fig. S2A-C). With the exception of the eye and heart, the first Mitf$^+$ cells appeared at E9.5, and their cell numbers expanded during the subsequent days

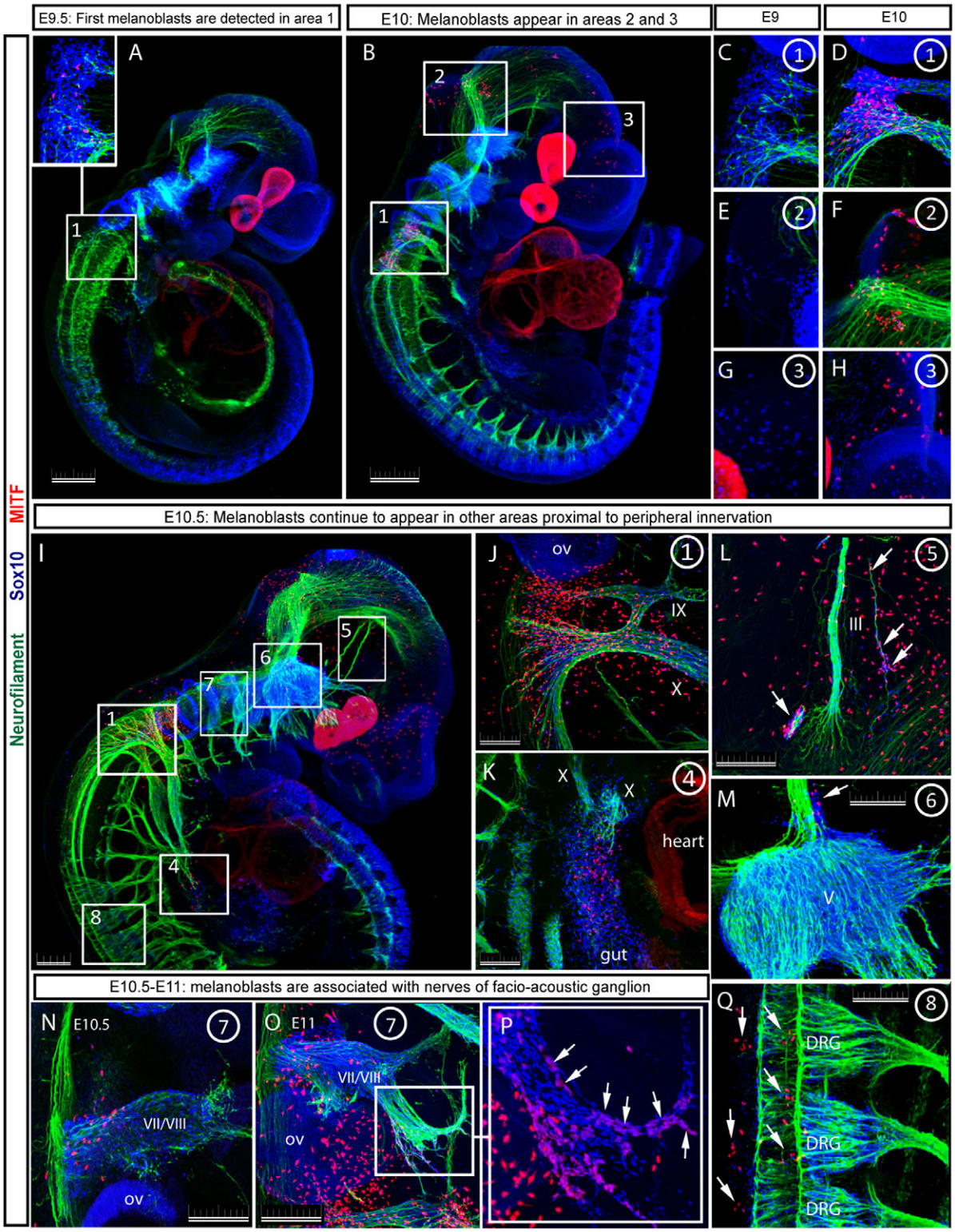

Fig. 2. Melanoblasts emerge in discrete and defined locations during mouse development. (**A**) Melanoblasts appear at E9.5 among Sox10$^+$ cells associated with roots of cranial ganglia IX-X (boxed area and enlarged image in inset). (**B**) At E10, melanoblasts are detected in three distinct locations:; adjacent to cranial nerves IX-X (box 1), in the midbrain-hindbrain region (box 2) and in the anterior facial region of the head (box 3). (**C-H**) Higher magnification of boxed areas 1 (C,D), 2 (E,F) and 3 (G,H). Note the presence of Sox10$^+$ cells in all three areas at E9 prior to emergence of Mitf$^+$ cells at E10. (**I-Q**) E10.5-11 embryos. (I) Overview of locations of Mitf$^+$ cells in the E10.5 embryo (boxed areas). (J-Q) Higher magnification images of boxed areas showing Mitf$^+$ cells in: (J) roots and nerves of cranial ganglia IX-X, (K) vagal nerve (X) innervating embryonic gut, (L) oculomotor nerve (III), (M) central root of the trigeminal ganglion, (N) the facio-acoustic ganglion complex, (O,P) branches of facial nerve (VIII), (Q) dorsal part of the embryo at the forelimb level between neural tube and roots of DRGs. Arrows point to some Mitf$^+$ cells. ov, otic vesicle. Roman numerals indicate the cranial nerves. Scale bars: 200 μm in A,B,I; 100 μm in J-Q.

of development (Fig. 1C-D, Fig. 2). Schematic illustrations of the appearance of Mitf$^+$ cells during embryogenesis are summarized in supplementary material Fig. S3.

In the nerve roots of cranial ganglia IX-X, few Mitf$^+$ cells were observed among many Sox10$^+$ cells at E9.5, but rapidly increased in number at E10 (Fig. 2A,B, boxed area 1 and Fig. 2C,D; supplementary material Fig. S2D-L, Movie 2). Mitf$^+$ cells were also observed at the midbrain-hindbrain border at E10 (Fig. 2B, boxed area 2 and Fig. 2E,F). At later stages, this cell cluster appeared to disperse, as a band of Mitf$^+$ cells was seen towards the head and face (Fig. 1, Fig. 2I; supplementary material Fig. S3). Scattered Sox10$^+$ cells were also observed at E9 in the anterior region of the head, and at E10 Mitf$^+$ cells appeared in this location without any apparent migration of Mitf$^+$ cells from the clusters located at the midbrain-hindbrain border or in the nerve IX-X, suggesting that some Mitf$^+$ cells differentiate from Sox10$^+$ cells of unknown segmental origin within the anterior head region (Fig. 2B, boxed area 3 and Fig. 2G,H; supplementary material Movie 3). Mitf$^+$ cells of the midbrain-hindbrain cluster and anterior part of the head were not associated with any nerves. At E10.5, Mitf$^+$ cells were dispersed in surrounding tissue of cranial nerves IX-X (Fig. 2J; supplementary material Fig. S2M-O, Fig. S4, Movies 4-6). These Mitf$^+$ cells appeared preferentially at the surface of nerves facing the skin (supplementary material Fig. S4). Apart from these major clusters of Mitf$^+$ cells, smaller numbers of Mitf$^+$ cells were found associated with cranial nerve III (Fig. 2I, boxed area 5 and Fig. 2L; supplementary material Movie 7), nerve V (Fig. 2I, boxed area 6 and Fig. 2M; supplementary material Movie 8) and nerves VII, VIII (Fig. 2I, boxed area 7 and Fig. 2N-P; supplementary material Movie 9). Mitf$^+$ cells were also observed in the gut and along vagal nerve fibers (Fig. 2I, boxed area 4 and Fig. 2K; supplementary material Movie 10). Dopachrome tautomerase$^+$ (Dct$^+$) cells and Kit$^+$ cells were also observed in nerves (supplementary material Fig. S5A-H) and these were found to always co-label with Mitf (supplementary material Fig. S5D-E,H), confirming a melanoblast phenotype of nerve-associated Mitf$^+$ cells. These melanoblasts (i.e. Sox10$^+$, Mitf$^+$, Dct$^+$ and Kit$^+$ cells) were also labeled by Tuj1 (Tubb3 – Mouse Genome Informatics), which stains class III β-tubulin, but were negative for PGP9.5 (Uchl1 – Mouse Genome Informatics), which labels neurons (supplementary material Fig. S5I-L). At E12.5, apart from distal parts of growing limbs and some parts in the neck region, the entire body of the embryo contained melanoblasts (data not shown). These results might indicate several different cellular origins of melanocytes in the head and neck. Those associated with nerves could be of SCP origin whereas others might originate directly from the NC, for instance those at the midbrain-hindbrain border and anterior part of the face that are first associated with clustered Sox10$^+$ cells independent of nerves.

The expression of Foxd3, which is a marker of NCCs and SCPs, was largely mutually exclusive with Mitf expression, and the rare colocalization of Mitf and Foxd3 in nerves often appeared fragmented (supplementary material Fig. S6A-G,M,N, Fig. S7A-I). Brain fatty acid binding protein (BFABP; Fabp7 – Mouse Genome Informatics), which is expressed in SCPs (supplementary material Fig. S6D-N, Fig. S7J-K) (Woodhoo et al., 2004; reviewed by Jessen and Mirsky, 2005) was present at varying levels in Mitf$^+$ melanoblasts located adjacent and proximally to cranial nerves (supplementary material Fig. S6H,I,K,L). Melanoblasts that were not close to peripheral nerves did not reveal Foxd3 or BFABP expression.

Distinct origins of cranial melanocytes

Inducible, tissue-specific genetic tracing was used to address the cellular and molecular origin of melanoblasts. For this, a transgenic strain in which the proteolipid protein (PLP) promoter drives a tamoxifen (TM)-inducible Cre recombinase (CreERT2) was employed, which is specifically expressed in SCPs and Schwann cells (Leone et al., 2003; Adameyko et al., 2009). As an indicator strain, *Rosa26-YFP* reporter was used; upon Cre-mediated recombination, a stop cassette is removed, and YFP is expressed in the cells that expressed Cre and in their daughters. TM was injected in *PLPCreERT2/Rosa26-YFP* mice at E9.5 when migration of cranial NCCs to the region of cranial nerves IX-X was complete but few Mitf$^+$ melanocytes could be observed (supplementary material Fig. S2A-F). Embryos harvested and analyzed one day later (i.e. E10.5) revealed YFP in Sox10$^+$ SCPs of the nerves and in Mitf$^+$ cells in and around cranial nerves (Fig. 3A-C). Quantification showed that 71.5±1.8% (n=4) of SCPs in nerves were successfully recombining upon TM injection. The percentage of Mitf and YFP double-positive melanoblasts was similar to the recombination frequency in SCPs (66.1±3.0%, n=4; Fig. 3G). We confirmed a specific and selective expression of Cre in SCPs by immunohistochemical staining for Cre. At E9.5, the stage when tamoxifen was injected for lineage tracing, Cre was exclusively expressed in SCPs of nerves and cells with high Cre had low or no Mitf expression (supplementary material Fig. S8A-C). Analysis of E10.5 embryos confirmed a strong negative correlation between Cre and Mitf expression and, at this stage, Mitf$^+$ melanoblasts were also located outside the cranial nerves and such cells were invariably negative for Cre (Fig. 3D-F,H; supplementary material Fig. S8D). Moreover, populations of Mitf$^+$ cells inside and outside the nerve showed similar proportion of YFP as result of recombination (supplementary material Fig. S8E). These results show that melanocytes appearing in and around cranial nerves IX-X originate from SCPs of these nerves.

Signals regulating development of cranial melanocytes

Neuregulin-1 signaling is required for proliferation, migration and survival of SCPs but suppresses melanocyte differentiation (Adameyko et al., 2009). If melanocytes around cranial nerves IX-X were to derive from SCPs we would expect to find an increase in melanocyte numbers at the expense of SCPs in *ErbB3*$^{-/-}$ mice. At E9.5 and E10.5, the vast majority of Sox10$^+$ SCPs were absent from the nerves *ErbB3*$^{-/-}$ mice, and a significant reduction in Mitf$^+$ cells was observed associated with the nerves compared with controls (Fig. 3I-Q; supplementary material Movie 11, Fig. S9A-D, arrows). We examined whether melanoblasts of cranial nerve IX-X depend on neuregulin-1 signaling by determining the proportion of Sox10$^+$/Mitf$^+$ melanoblasts and Sox10$^+$/Mitf$^-$ SCPs among all Sox10$^+$ cells at E10.5. Despite the massive reduction in the absolute numbers of SCPs, a disproportionately high number of Mitf$^+$ melanoblasts were observed around ganglia and nerves IX-X in *ErbB3*$^{-/-}$ mice (Fig. 3R). Hence, the vast majority of the remaining Sox10$^+$ cells in *ErbB3*$^{-/-}$ mice had adopted a melanocyte fate. Importantly, Mitf$^+$ cells scattered in the midbrain-hindbrain and anterior head of *Erbb3*$^{-/-}$ mice of E10.5 embryos were not different from *Erbb3*$^{+/+}$ littermate controls (supplementary material Fig. S9E,F arrows and Fig. S9G). This shows that development of only nerve-derived melanocytes is affected by neuregulins.

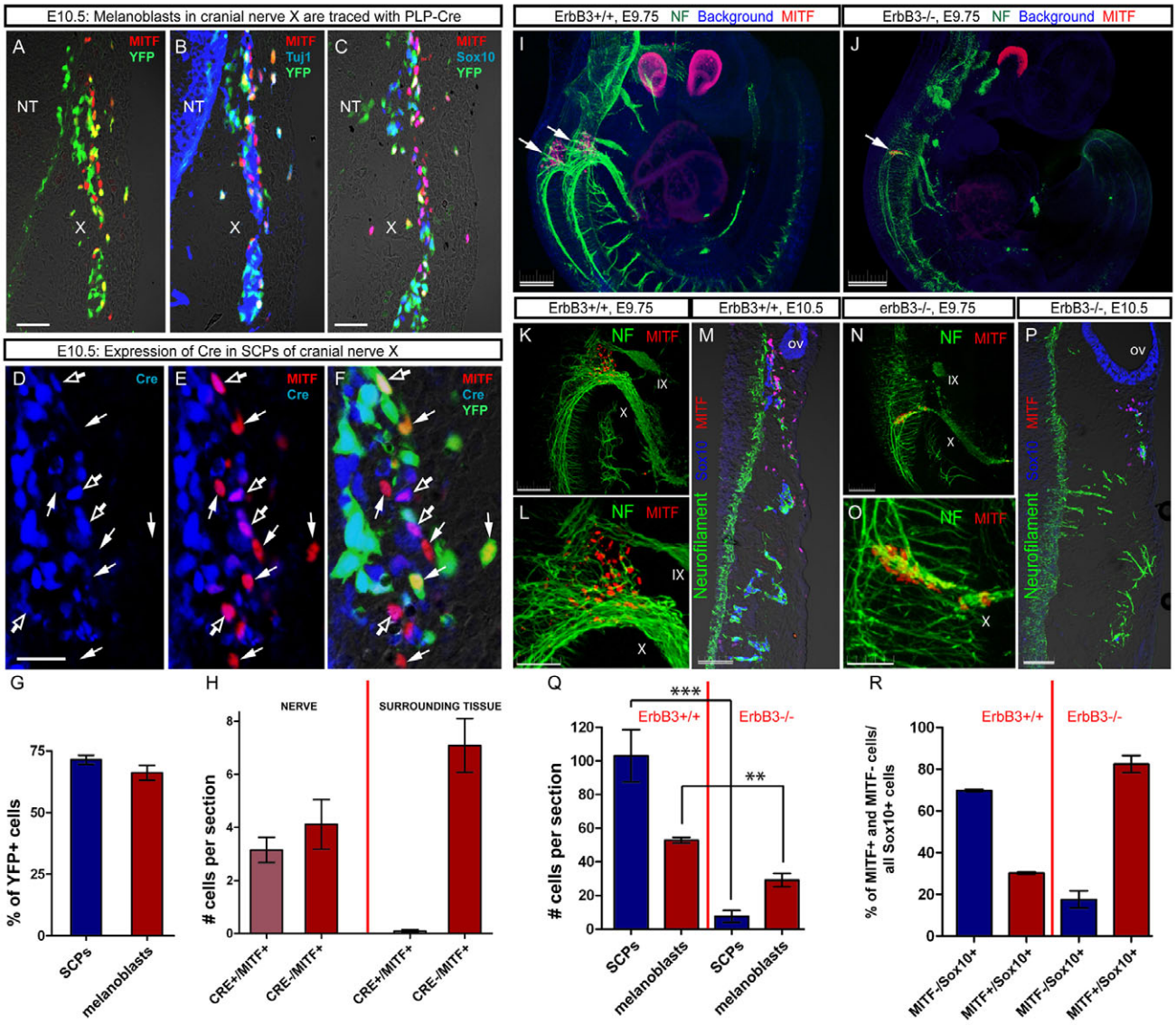

Fig. 3. Genetic tracing using *PLP-CreERT/Rosa26-YFP* mice and analysis of neuregulin receptor subunit (*Erbb3*) mutant mice reveal SCP-derived melanoblasts in cranial nerves IX-X. (**A-C**) Injection of TM at E9.5 and analysis at E10.5 of Mitf and YFP (A); Mitf, Tuj1, YFP (B); and Mitf, Sox10, YFP (C). Note the presence of YFP in a significant proportion of Mitf$^+$ cells in the Tuj1$^+$ and Sox10$^+$ nerve and in Mitf$^+$ cells associated with but not within the nerve. (**D-F**) Immunohistochemical staining for Cre recombinase, Mitf and YFP in PLP-CreERT2 mice at E10.5. Note the expression of Cre in SCPs of nerves, including those that are weakly Mitf$^+$ within nerves (unfilled arrows), but not in strong Mitf$^+$ cells (filled arrows). (**G**) Quantification of YFP$^+$ cells in Sox10$^+$ SCPs of nerves and in Mitf$^+$ melanoblasts (n=4). (**H**) Quantification of Cre expression in Mitf$^+$ cells in SCPs of nerves and melanoblasts outside cranial nerves IX-X. (n=4). (**I**,**J**) Whole-mount immunohistochemistry of E9.75 wild-type (I) and *ErbB3*$^{-/-}$ (J) mouse embryos stained for NF (green) and Mitf (red). Arrows indicate clusters of melanoblasts associated with cranial nerves IX-X. (**K**,**L**) Cranial nerves IX-X of an E9.75 *ErbB3*$^{+/+}$ embryo. (**M**) Cross-section through cranial nerves IX-X of an E10.5 *ErbB3*$^{+/+}$ embryo. Note the numerous Sox10$^+$ SCPs and Mitf$^+$ melanoblasts associated with NF$^+$ nerve fibers. (**N**,**O**) Cranial nerves IX-X of an E9.75 *ErbB3*$^{-/-}$ embryo. (**P**) Cross-section through cranial nerves IX-X of an E10.5 *ErbB3*$^{-/-}$ embryo. Note the reduction of Sox10$^+$ SCPs and Mitf$^+$ melanoblasts. (**Q**) Cell numbers of SCPs and melanocytes in wild-type and *ErbB3*$^{-/-}$ E10.5 embryos (***P=0.001, n=4 embryos/genotype). (**R**) Percentage of melanoblasts (Sox10$^+$:Mitf$^+$) and SCPs (Sox10$^+$:Mitf$^-$) relative to all Sox10$^+$ cells in wild-type and *ErbB3*$^{-/-}$ E10.5 embryos. Note that the proportion of Mitf$^+$ cells is much higher in *ErbB3*$^{-/-}$ than in wild-type embryos. Error bars represent s.e.m. Red line in H, Q and R separates analyzed tissues or genotypes. NT, neural tube; ov, otic vesicle. Roman numerals indicate the cranial nerves. Scale bars: (A-C) 50 μm inA-C; 30 μm in D-F; 250 μm in I,J; 100 μm in K,M,N,P; 50 μm in L,O.

The emergence of melanocytes in discrete locations points towards the presence of specific soluble ligands inducing and/or expanding melanoblasts locally. To address this we analyzed Mitf-, Sox10- and NF- expressing cells in endothelin receptor B mutant (Ednrb$^{-/-}$ and Ednrb$^{+/-}$) mice. Mitf$^+$ cells around cranial nerve IX-X were greatly diminished and appeared to be attached to the nerve fibers, with few cells dispersing into the surrounding tissue (Fig. 4A-D,F-I; supplementary material Fig. S10A,B) and were completely absent around nerves III, V and VII-VIII (supplementary material Fig. S10C,D). By contrast, midbrain-hindbrain Mitf$^+$ cells did not display any deficit of dispersal and the impact on cell numbers was moderate compared with nerve IX/X (Fig. 4E,J,K). Expression of endothelin 3 (*Edn3*) mRNA was present in the otic vesicle, weakly expressed in tissues

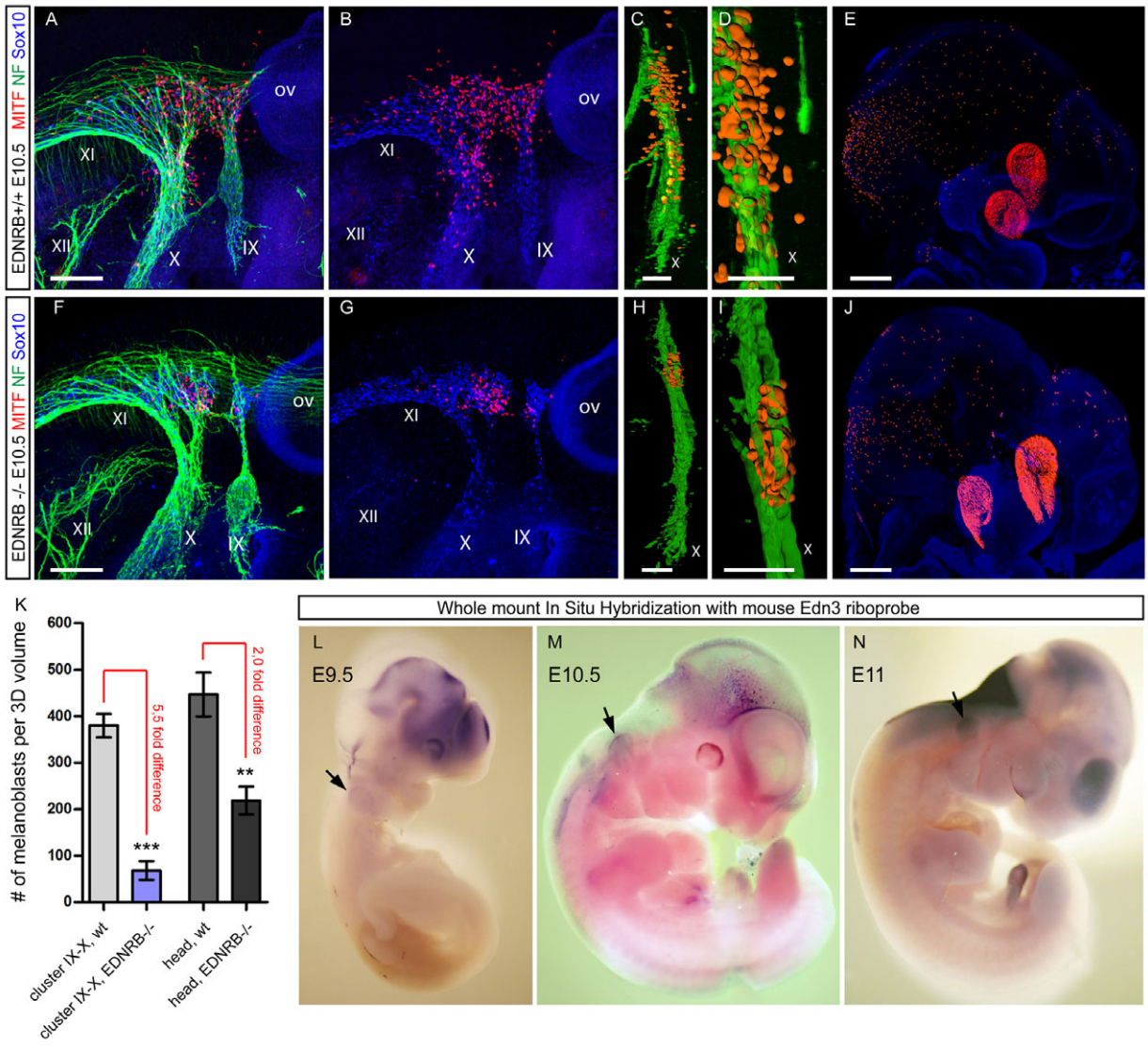

Fig. 4. Distinct roles of endothelin 3 for nerve IX/X and midbrain-hindbrain melanoblasts. (**A-E**) Cervical cluster of melanoblasts (A-D) and the whole head (E) of a wild-type control mouse embryo. Note that the cervical part of E10.5 embryo is also represented by 3D-rendered isosurfaces of cranial nerves IX-X (green) together with melanoblasts (orange) shown in transversal view in C and D. (**F-J**) Cervical cluster of melanoblasts (F-I) and the whole head (J) of an *EDNRB*$^{-/-}$ embryo at E10.5. Note deficits of dispersal and expansion of melanoblasts associated with cranial nerves whereas only expansion is affected in midbrain-hindbrain melanocytes of *EDNRB*$^{-/-}$ mutant embryos. (**K**) Quantification showing decreases of melanoblast numbers in the cervical cluster and scattered in the head compared with littermate controls at E10.5 (***P=0.0003, n=4 animal/genotype for cluster IX-X; **P=0.0011, n=4 animal/genotype for the whole head). Error bars represent s.e.m. (**L-N**) Whole-mount in situ hybridization with *Edn3* riboprobe on mouse embryos at E9.5 (L), E10.5 (M) and E11 (N). Note the expression of Edn3 in otic vesicle (arrows). ov, otic vesicle. Roman numerals indicate the cranial nerves. Scale bars: 100 μm in A,B,F,G; 50 μm in C,D,H,I; 300 μm in E,J.

surrounding cranial ganglia IX-X and VII/VIII and expressed in midbrain-hindbrain at E9.5-11.0 (Fig. 4L-N). Analysis of Wnt5a-null mutant (Wnt5a$^{-/-}$) mice revealed a decrease of Mitf^{+} cells in nerve IX/X cluster, but dispersal was not affected (supplementary material Fig. S11). These results show that Ednrb and Wnt5a are necessary for expansion and Ednrb for migration of SCP-derived melanoblasts.

Cross-regulatory interactions of Sox2 and Mitf determine cell fate choice in the neural crest

We noticed a defined pattern of Sox2 expression during NC development. Upon completion of NCC migration, Sox2 was detected in SCPs covering peripheral nerves and in satellite cells of sensory ganglia (Fig. 5A, Fig. 6C,E-G; supplementary material Fig. S12A-I), as previously shown (Wakamatsu et al., 2004). Intriguingly, Sox2 levels progressively declined in a proximal to distal direction along the length of peripheral nerves of both chick and mouse (Fig. 5A, Fig. 6E). Sox2 was also clearly detected in SCPs of nerve fibers from which melanoblasts emerged, including the brachial plexus at E4.5 in chick embryos (Fig. 5B,C), cranial nerves at E10.5 (Fig. 6A-D) and dorsal rami nerves at in mouse embryos at E12 (Fig. 6F,G). Mitf^{+} and Sox2^{+} cells were mutually exclusive outside nerves and partially exclusive within nerves where double-labeled cells within nerves often contained high levels of Sox2 concomitant with low levels of Mitf and vice versa (Fig. 5A, inset, Fig. 5B-E, Fig. 6A-D, Fig. 6C,D, yellow arrows).

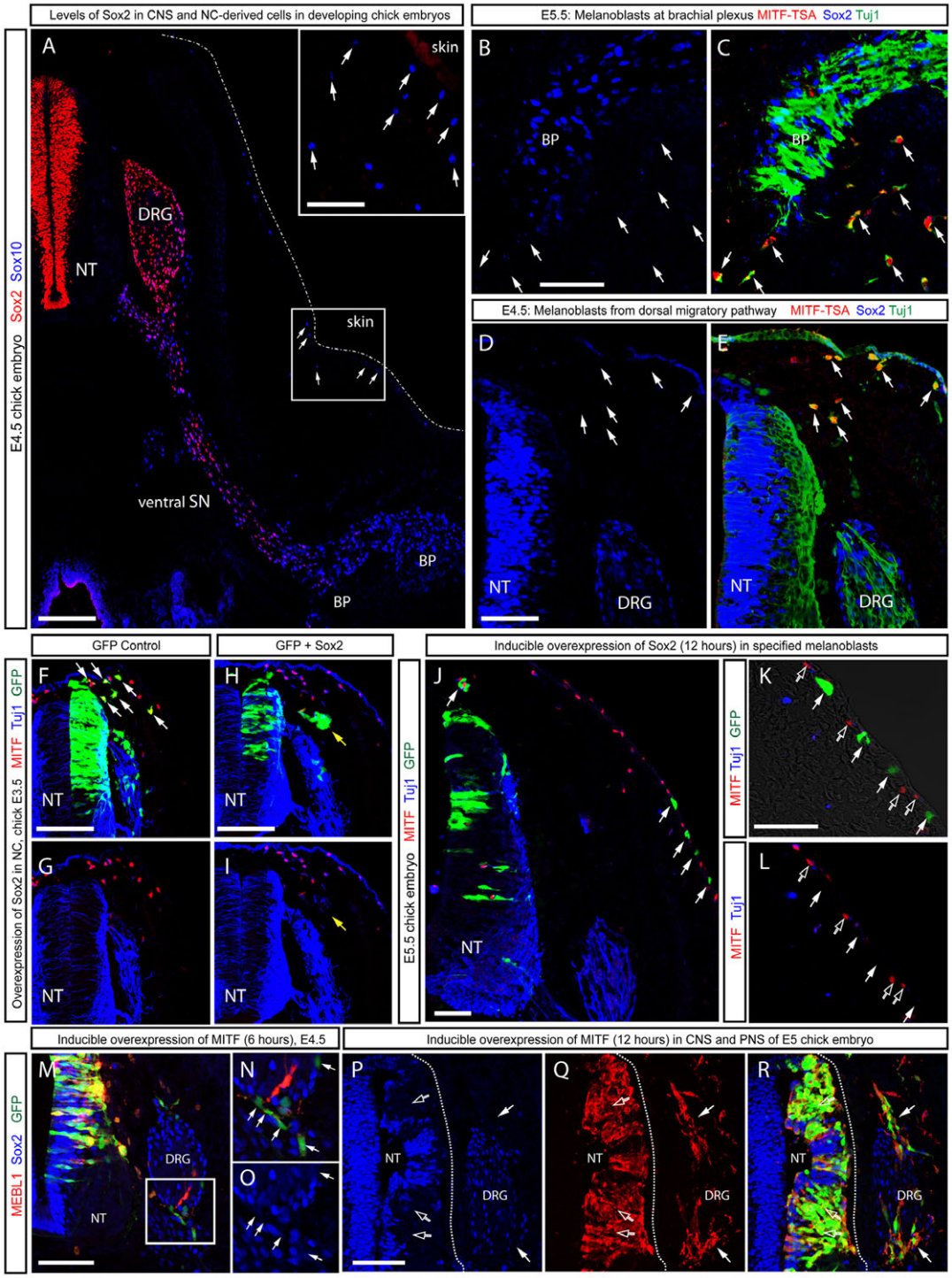

Fig. 5. Sox2 and Mitf cross-regulatory interactions during melanocyte development in chick. (**A**) Cross-section through the forelimb level of E4.5 chick embryo stained for Sox2 (red) and Sox10 (blue). Boxed area is enlarged in inset. Note the lack of Sox2 expression in Sox10^{+} cutaneous melanocytes (arrows) and the gradual reduction of Sox2 in more distal parts of the ventral spinal nerve. (**B**,**C**) Mitf, Sox2 and Tuj1 staining of the brachial plexus. Sox2^{+} is observed in SCP whereas Mitf^{+} melanoblasts lack Sox2 (arrows). (**D**,**E**) Mitf, Sox2 and Tuj1 staining of the dorsal neural tube. Note the lack Sox2 immunoreactivity in the nuclei of NCC-derived Mitf^{+} cells (arrows) at E4.5. (**F-I**) NC overexpression of Sox2 and GFP in the chick. GFP labels overexpressing cells. In control GFP-overexpressing embryos, GFP labeled cells are observed among melanoblasts (Mitf^{+} cells) and the DRG (arrows). Sox2 expression leads to loss of GFP^{+}/Mitf^{+} cells (white arrows) and ectopic ganglia-like formations (yellow arrows). (**J-L**) Inducible overexpression of Sox2 and GFP at E5.0 in the chick with analysis 12 hours later. Non-overexpressing melanoblasts (i.e. GFP^{-} cells) contain Mitf (unfilled arrows) whereas GFP^{+} cells completely lack Mitf immunoreactivity (filled arrows). (**M-O**) Inducible overexpression of Mitf for 6 hours caused significant repression of Sox2 in targeted (GFP^{+}) cells (arrows) in CNS and PNS, and weak ectopic Mebl1 expression in spinal cord. N and O are high magnification images of the boxed area in M. (**P-R**) Inducible overexpression of Mitf for 12 hours caused a complete loss of Sox2 in targeted cells in CNS (unfilled arrows) and PNS (filled arrows) (P). Ectopic expression of Mebl1 was observed in overexpressing (GFP^{+}) cells (Q). Dotted line outlines the neural tube. BP, brachial plexus; SN, ventral spinal nerve; NT, neural tube. Scale bars: 150 μm in A; 70 μm in A, inset; 50 μm in B,C; 100 μm in D-R.

Next, we addressed the function of Sox2 and Mitf for specification of melanocytes in gain- and loss-of-function experiments. Sox2 and green fluorescent protein (GFP) expression plasmids were electroporated in ovo at E2 identifying electroporated cells by GFP fluorescence. Forced expression of Sox2 led to reduced NC delamination, appearance of ectopic ganglia-like structures dorsal of the DRG similar to those observed in a previous study (Wakamatsu et al., 2004) (Fig. 5H-I, yellow arrows; supplementary material Fig. S13A, white arrows), and Mitf expression was very rarely observed (2 of 210 dorsolateral migratory GFP$^+$ cells were Mitf$^+$, *n*=10 embryos) unlike in control embryos expressing only GFP (124 of 184 dorsolateral migratory GFP$^+$ cells were Mitf$^+$, *n*=10 embryos) (Fig. 5F-G).

Because forced Sox2 expression inhibits delamination of NCCs, the above phenotype on melanocyte development could be indirect. To allow melanocyte migration and differentiation prior to Sox2 expression, we electroporated E2 chick embryos with a single DNA construct containing both GFP and *Sox2* genes under the control of identical doxycyclin-inducible promoters. *Sox2* and GFP were activated by the addition of doxycyclin at E5, when specification and migration of melanoblasts is complete. Embryos were collected 12 hours after induction of Sox2 and GFP expression. Immunohistochemical staining confirmed the successful expression of Sox2 (supplementary material Fig. S13C). In these experiments, Sox2$^+$/GFP$^+$ melanoblasts located in the embryonic epidermis did not contain nuclear Mitf (0/63 GFP$^+$ cells contained Mitf, *n*=4 embryos) (Fig. 5J-L) or cytoplasmic immunoreactivity using the Mebl1 antibody, which specifically recognizes avian melanocytes (supplementary material Fig. S13D-F), unlike neighboring untransfected GFP$^-$ melanoblasts, which always co-expressed Mitf and Mebl1 (Fig. 5K,L, unfilled arrows; supplementary material Fig. S13F, unfilled arrows). By contrast, after inducible overexpression of only GFP in committed melanoblasts, 71 out of 71 GFP$^+$ cells in the subepidermal space expressed Mitf, (supplementary material Fig. S13B, arrows, *n*=4 embryos). Hence, the presence of Sox2 in SCPs of nerves and its ability to rapidly and robustly downregulate Mitf in differentiating and already established melanocytes of the chick show that Sox2 expression is incompatible with the melanocyte fate.

We next examined loss of function of Sox2 in conditional mutant (Favaro et al., 2009) (Sox2$^{fl/fl}$) mice crossed to Wnt1-Cre, which produces a reliable recombination and inactivation of genes in the NC (Danielian et al., 1998). Wnt1Cre/Sox2$^{fl/fl}$ mice did not have any gross abnormalities in the NC as seen by Sox10 staining at E9-10.5 and did not display precocious Mitf$^+$ cells in E9-9.5 embryos (Fig. 6I,K; supplementary material Fig. S14) and, hence, any phenotype of Mitf$^+$ cells at later stages should not be a consequence of an unexpected early NCC conversion to melanoblasts. A nearly twofold increase of Mitf$^+$ cells associated with cranial nerves IX-X was seen at E10.5 (Fig. 6I-Q; supplementary material Fig. S15H-K) and a less pronounced but still significant increase at E11.0 (supplementary material Fig. S15A-C). Similar results were obtained for Mitf$^+$ cells adjacent to cranial ganglia V, VII/VIII at E10.5 (Fig. 6R; supplementary material Fig. S15D-G). Furthermore, the proportion of Mitf$^+$/Sox10$^+$ cells around nerves IX-X was increased in Wnt1Cre/Sox2$^{fl/fl}$ mice (Fig. 6Q), without any difference in the total number of Sox10$^+$ cells (914±62 and 871±54, wild-type and Wnt1Cre/Sox2$^{fl/fl}$ mice, respectively, *n*=4/genotype). Consistently, Sox10$^+$/Mitf$^-$ SCPs decreased (526±50 and 294±36, wild-type and Wnt1Cre/Sox2$^{fl/fl}$ mice, respectively, *n*=4/genotype) (Fig. 6P), confirming that the increase in melanoblast numbers occurs at the expense of glial fate in the absence of Sox2 in SCPs. Because Sox2 is ablated in NCCs, there could be an effect on a putative neural crest cell/bipotent glia-melanocyte progenitor prior to glial fate acquisition rather than a glia to melanocyte transition. However, this would be inconsistent with the numbers of Sox10$^+$ and Mitf$^+$ cells observed. Analysis of pigmentation in Wnt1Cre/Sox2$^{fl/fl}$ mice at postnatal stage (P) 5 revealed no increase in skin color and melanocyte numbers in hair follicles of the back skin (supplementary material Fig. S15L-M).

The results described above show that Sox2 can suppress Mitf and that in the absence of Sox2, more Mitf$^+$ cells develop. To examine whether Sox2 and Mitf have cross-repressory functions during fate determination of SCPs in nerves, we investigated whether Mitf regulates *Sox2*. For this, we established a doxycyclin-inducible Mitf and GFP overexpression construct. This plasmid or a control GFP inducible plasmid was electroporated in the chick neural tube of E2 embryos, doxycyclin was added at E4.5, and embryos were harvested six and twelve hours after doxycyclin addition (E4.75 and E5). We confirmed Mitf expression upon induction (supplementary material Fig. S13G) and observed no effect of the GFP-only vector on Sox2 or Mitf expression in control embryos (supplementary material Fig. S13B,H-L). However, inducible expression of Mitf led to rapid repression of Sox2. This was already observed after six hours in the neural tube and neural crest and its derivatives, i.e. in neuronal progenitors and neurons of the neural tube and the periphery, in border cells, satellite cells and SCPs (Fig. 5M-O; supplementary material Fig. S13M-Q). After 12 hours of Mitf expression, Sox2 was completely absent in virtually all electroporated cells, and Mebl1 was expressed ectopically in both the peripheral and central nervous system (Fig. 5P-R; supplementary material Fig. S13R-V). Next, we examined Mitf loss of function. Electroporation of two different siRNAs for Mitf led to an efficient downregulation of Mitf, and their combination produced an even stronger effect compared with scrambled siRNA control (supplementary material Fig. S16A-J). In the siRNA condition, both GFP$^+$/Mitf$^+$ and GFP$^+$/Sox2$^-$ cells in the NC lineage demonstrated a strong decrease in numbers in the Mitf siRNA1+2 condition whereas the total numbers of electroporated GFP$^+$ cells in the NC lineage did not change (supplementary material Fig. S16J,K). This result suggests that Sox2 failed to be repressed in Sox2$^+$ NCCs when Mitf activity was attenuated.

Sox2 acts as a repressor on the *Mitf* proximal promoter

Our results opened for that Sox2 might be regulating *Mitf* directly by binding to its promoter region. The genomic organization of the *Mitf* gene is highly conserved between mice and humans. Among the different promoter elements, the melanocyte-specific Mitf-m promoter has shown to be regulated by several transcription factors, including Sox10, Lef-1, Pax3 and CREB (Steingrimsson et al., 2004) (Fig. 7A). A computer-based DNA sequence analysis by JASPAR (Sandelin et al., 2004) (http://jaspar.genereg.net/) revealed two putative Sox2 binding sites at Mitf-m proximal promoter (Fig. 7A, gray boxes). Chromatin immunoprecipitation assays performed on mouse embryonic stem (ES) cells, which express Sox2 at high levels, showed that Sox2 binds preferably at the most proximal binding site of the Mitf-m promoter, supporting a direct role of Sox2 as a regulator of *Mitf* expression (Fig. 7A,B).

We used a luciferase reporter assay to address whether Sox2 can regulate the activity of the proximal Mitf-m promoter in vitro. Expression plasmids for Sox2 and the *Renilla* luciferase reporter driven by the proximal promoter of Mitf-m were introduced into B16-F10 cells (Thomas and Erickson, 2009).

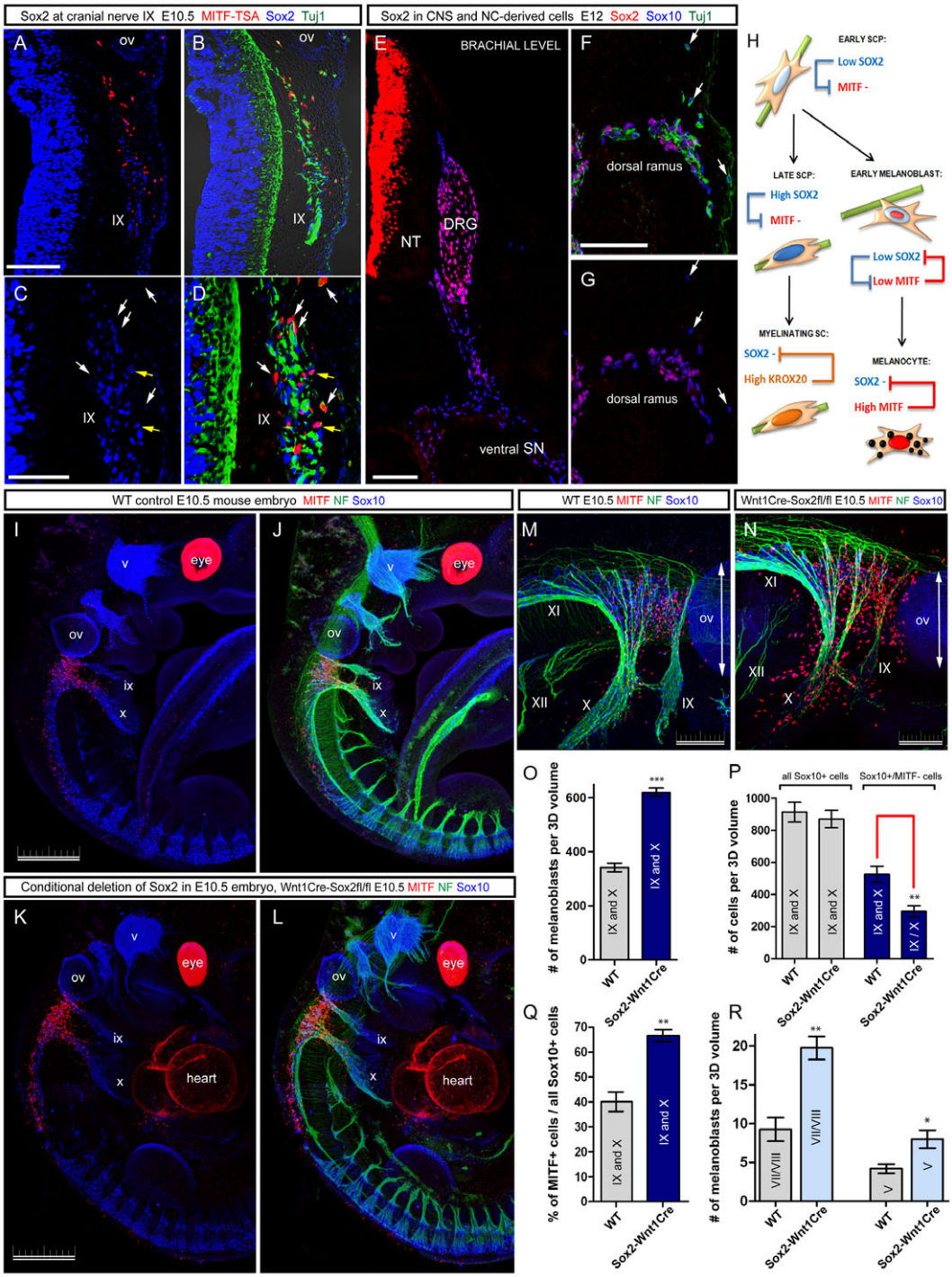

Fig. 6. Sox2 regulatory effects on melanocyte development in NCC conditionally mutant mice (*Wnt1Cre/Sox2$^{fl/fl}$*). (**A-D**) Expression of Sox2 (blue) and Mitf (red) in cells associated with cranial nerve IX in E10.5 mouse embryos. White arrows point at Mitf^{+} cells with no or very low levels of Sox2 (C,D), yellow arrows show Mitf^{+} cells retaining low levels of Sox2 (C,D). (**E**) Sox2 expression (red) decreases proximo-distally in the ventral spinal nerve (SN) in the E12 mouse embryo. (**F**,**G**) Sox2 expression in SCPs of spinal nerve dorsal rami. Arrows indicate Sox10^{+} prospective melanoblasts under the epidermis that are negative for Sox2. (**H**) Schematic model of *Sox2* and *Mitf* cross-repressive interactions during development of the glial and melanocyte lineages. (**I-L**) Conditional deletion of *Sox2* in the NCCs using the *Wnt1-Cre* activator strain. Melanoblasts numbers at the cranial nerves IX-X cluster markedly increased in conditional null mice (K,L) compared with control mice (I,J). (**M**,**N**) Magnified view of part of J and L. (**O**) Quantification of Mitf^{+} cells in IX-X cluster of wild-type and *Wnt1Cre/Sox2$^{fl/fl}$* mice at E10.5 (left graph, $P<0.0001$, $n=4$). (**P**) Quantification of all Sox10^{+} cells and Sox10^{+}/Mitf^{-} cells in cranial nerves IX/X of *Wnt1Cre/Sox2$^{fl/fl}$* and wild-type embryos (for Sox10^{+}/Mitf^{-} cells $^{**}P=0.0096$, $n=4$ embryos/genotype). (**Q**) Percentage of Mitf^{+}/Sox10^{+} cells among all Sox10^{+} cells between *Wnt1Cre/Sox2$^{fl/fl}$* embryos and littermate wild-type embryos ($^{**}P=0.0012$, $n=4$ embryos/genotype). (**R**) Quantification of melanoblasts appearing adjacent to cranial ganglia V and VII/VIII in *Wnt1Cre/Sox2$^{fl/fl}$* embryos and littermate control embryos (ganglion V: $^{*}P=0.0161$, $n=3$ *Wnt1Cre/Sox2$^{fl/fl}$* and $n=5$ in control; ganglia VII/VIII: $^{**}P=0.0014$, $n=4$ *Wnt1Cre/Sox2$^{fl/fl}$* and $n=8$ in control). (O-R) Error bars represent s.e.m. NT, neural tube; ov, otic vesicle; SN, ventral spinal nerve. Roman numerals indicate the cranial nerves. Scale bars: 100 μm in A,B,F,G,M-P; 50 μm in C,D; 500 μm in I-L.

Overexpression of Sox10 was used as a positive control, and the absence of overexpression plasmid was used as a negative control. The data were normalized for transfection efficiency by measuring the activity of a second reporter plasmid carrying Firefly luciferase. Sox2 was found to robustly downregulate Mitf promoter activity whereas Sox10, similar to controls, had no effect (Fig. 7A,C,D). We next addressed whether such downregulation of Mitf results from a direct repressor function of Sox2 using constructs containing the DNA-binding domain of Sox2 coupled to either a strong transcriptional repressor, engrailed (Sox2-ENR), or a transcriptional activator, VP16 (Sox2-VP16) (Fig. 7C). Experiments were conducted as described for the wild-type Sox2 construct. Sox2-ENR led to a marked downregulation of promoter activity, similar to that observed with full length Sox2, whereas Sox2-VP16 resulted in a small but significant decrease (Fig. 7D). These in vitro data using Sox2-ENG and Sox2-VP16 constructs were confirmed in vivo using chicken electroporation. A GFP plasmid used as a control demonstrated the presence of $GFP^+/Mitf^+$ melanoblasts migrating in the dorsolateral pathway (Fig. 7E,F, arrows). The introduction of Sox2-ENR led to a complete absence of Mitf in all targeted cells (Fig. 7G,H, arrows) similar to observations in the Sox2 overexpression experiment (Fig. 6G,H). Overexpression of Sox2-VP16 caused detectable expression of Mitf in all targeted GFP^+ cells (Fig. 7I,J, arrows). The level of Mitf in targeted cells was weak compared with Mitf in non-targeted migratory melanoblasts. In addition, an ectopic expression of Mitf localized to the nuclei was observed in the neural tube starting from E3.5 and increasing at E4.5 (Fig. 7I-L, unfilled arrows). We suggest that the small reduction of reporter activity using Sox2-VP16 might be caused by a displacement of Mitf activators in Mitf-expressing cells. Additionally, we propose that the weak ectopic expression of Mitf in vivo in cells that normally do not express Mitf was a result of the artificial transactivating activities of VP16. Hence, these results confirm direct repressive binding of Sox2 to Mitf promoter.

DISCUSSION

In this report, we show that melanocytes in the head and neck arise from several different progenitor cell types, including nerve-derived SCPs and presumptive NCCs. The earliest melanoblasts in the developing mouse embryo are nerve-derived and originate at E9.5 from SCPs sitting in roots of IX-X cranial nerves. This anatomical structure produces large quantities of melanoblasts between E9.5 and E11 of mouse development by a mechanism that is dependent on signaling from Ednrb and Wnt5a. On the contrary, melanoblasts that emerge at the midbrain-hindbrain border and later appear in an anterior band of cells are not associated with nerves and, hence, might differentiate directly from NCCs. Our results also show that Sox2 expression is strictly controlled in a proximo-distal manner in nerves. Sox2 and Mitf cross-regulate each other providing a mechanism that participates in determining melanoblast cell fate.

Cellular origin, migratory paths and signals regulating fate and expansion of cranial melanocytes

The expression of melanocyte markers Mitf, Dct, Pml17 and the stem cell factor receptor Kit has previously been used to delineate development of cranial melanocytes (Alizadeh et al., 2008; Baxter and Pavan, 2003; Bernex et al., 1996; Jordan and Jackson, 2000a; Mackenzie et al., 1997; Wilkie et al., 2002; Wilson et al., 2004). In *Dct-lacZ* embryos, labeled cells cluster in the cervical neck region as early as E10.5. At E11.5, this cluster is still evident but cells are also observed at the dorsal aspect of the eye, suggesting that head and face melanocytes arise from the cervical neck region and migrate laterally towards the eye and face (Jordan and Jackson, 2000a; Wilkie et al., 2002). Although Dct is an early marker for melanocytes, it is expressed later than Pme17 and Kit. Pme17 expression is observed at E10.5 in cells that extend from the midbrain-hindbrain boundary laterally and rostrally towards the eye (Alizadeh et al., 2008; Baxter and Pavan, 2003). Melanocytes at the midbrain-hindbrain and cervical clusters have been detected previously using *c-Kit-lacZ* mice (Wilson et al., 2004). Our study here indicates that these two clusters of melanoblasts correspond to the main sites of emergence of melanocytes, and we propose that these sites represent the major source of head and neck pigment cells. Although the midbrain-hindbrain cluster of melanoblasts does not associate with any nerve, the cervical cluster is tightly associated with cranial nerves IX-X. We also report minor contributions of melanoblasts arising from SCPs associated with fibers of the trigeminal, facio-acoustic ganglia and the oculomotor nerves.

The large contribution and close association of melanocytes with cranial nerves IX-X led us to examine the origin of these cells in detail and compare their dependence on environmental signals for specification and expansion with that of midbrain-hindbrain melanocytes. Analysis of the entire embryonic body with cellular resolution using 3D imaging indicates that NC migration in the cranial region is complete by E9.5, when cranial nerve IX-X-associated melanoblasts first appear in the embryo. Hence, melanoblasts appearing inside nerves IX-X can only arise either from SCPs, or from NCCs that arrested migration in the nerves prior to commitment to a melanocyte fate. The close association of these cells with nerves suggests an SCP origin. Consistently, Bfabp was expressed in SCPs and also weakly in $Mitf^+$ cells associated with nerves but not in migrating NCCs and distal melanocytes, suggesting its downregulation in newly committed melanoblasts. Because SCPs, but not NCCs, depend on neuregulin signaling for their survival, the observation that melanoblast numbers of cranial nerves IX-X cluster were affected whereas midbrain-hindbrain melanoblasts were unaffected in $ErbB3^{-/-}$ mice further supports the notion of distinct cellular origins of these two populations. Furthermore, although the cranial nerves IX-X cluster critically depends on Ednrb for both expansion and dispersion, midbrain-hindbrain melanoblasts dispersed independently with moderate reductions in numbers. Finally, *PLP-Cre* cell-lineage tracing confirmed that melanoblasts of nerves IX-X were originating from SCPs. We find that melanoblasts derived from nerves IX-X are born mostly on the lateral side of these cranial nerves, i.e. at the position that faces the epidermis. Our interpretation of this data is that between E10 and E10.5 melanoblasts lose contact with the nerve, scatter and migrate laterally towards the ectoderm. The stereotypical anatomical locations and the distinct lateral migration towards the ectoderm suggest the presence of instructive signals and/or chemoattractants emanating from the epidermis.

Signals within the epidermis might be responsible for specifying the initial small numbers of melanocytes and/or such signals might instead expand and attract a small melanoblast cell pool that was specified by factors localized to the nerves. Although the failure of eliminating all $Mitf^+$ cells in mouse mutants for growth factors and morphogens could be a result of redundancy, our previous (Adameyko et al., 2009) and present data suggest that signals within the nerve might be sufficient for inducing $Mitf^+$ cells. Pdgf from nerves promotes a melanocyte fate whereas neuregulin-1

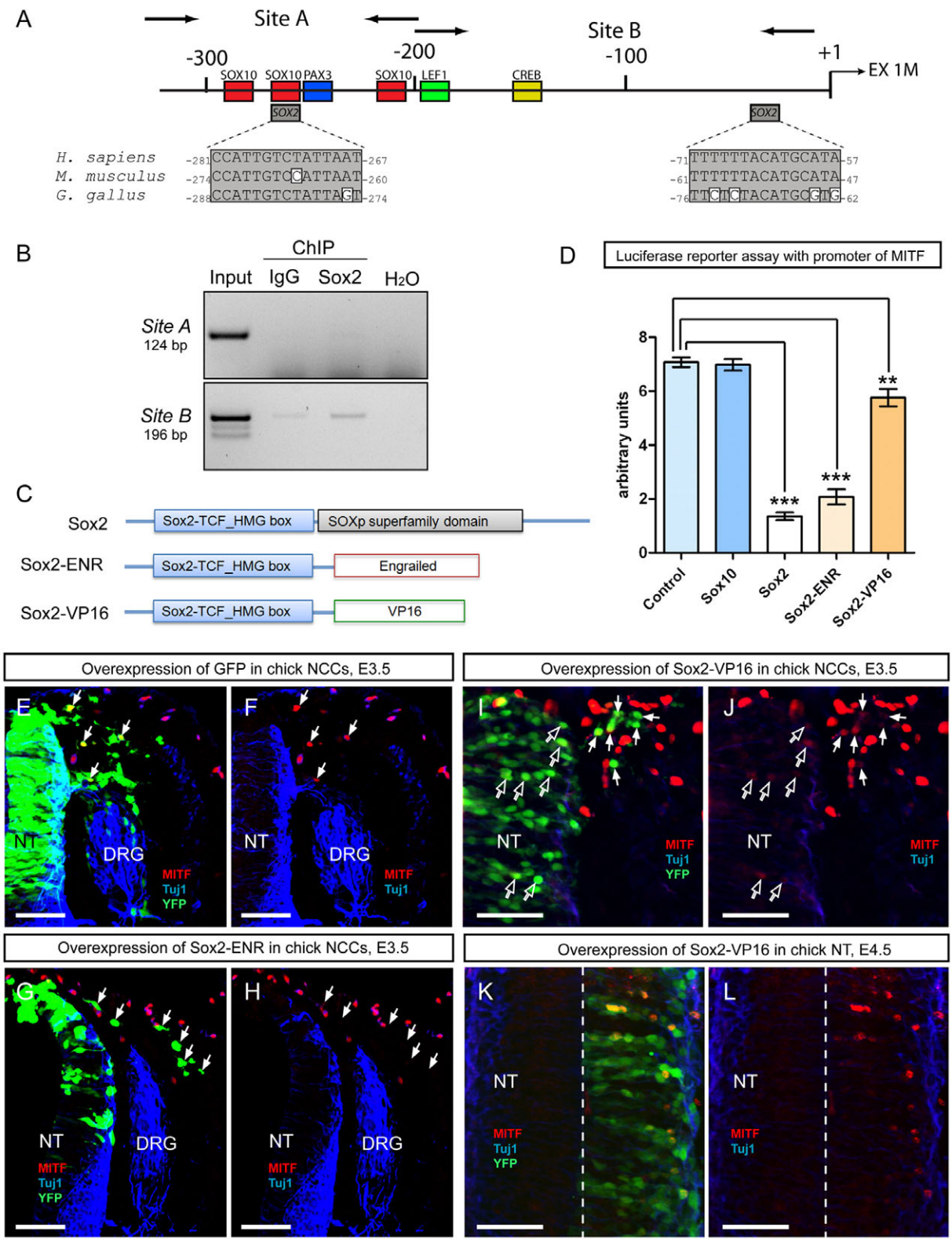

Fig. 7. Sox2 regulates the activity of Mitf-m proximal promoter. (**A**) Structure of Mitf-m proximal promoter with predicted binding sites. Arrows show the positions of primers used to amplify site A and site B in ChIP assay with Sox2 antibody. (**B**) PCR reaction demonstrating binding of Sox2 on the proximal Mitf-m promoter in ChIP assay. (**C**) Domain structure of Sox2 and Sox2-activating and -repressing fusion proteins used for overexpression experiments in vitro and in vivo. (**D**) Luciferase reporter assay in melanoma cells with endogenous Mitf-m promoter activity (control, n=16 vs: Sox2, n=8, ***P<0.0001; Sox2-ENR construct, n=8, ***P<0.0001; Sox2-VP16 construct, n=4, **P=0.0038). (**E-L**) In vivo effects of Sox-ENG and Sox2-VP16 on melanocyte development 2 days after electroporation in chick. Arrows in E,F,I,J show GFP$^+$/Mitf$^+$ migratory cells and in G,H, all GFP$^+$ cells. Solid arrows show NCC-derived cells, whereas open arrows point to cells in the neural tube. (K,L) Dashed line separates two halves of a neural tube. Note the presence of nuclear Mitf (red) in GFP$^+$ cells of the electroporated half. NT, neural tube. Scale bars: 100 μm.

suppresses a melanocyte fate and promotes Schwann cell differentiation (Adameyko et al., 2009; Jessen and Mirsky, 2002). Hence, such nerve-derived signals could induce an initially small pool of melanoblasts that expands under the influence of Wnt5a and Ednrb signaling. We speculate that the discrete locations of *endothelin 3* expression might be responsible for expanding melanocyte progenitors only at the sites of major clusters, making cranial nerves IX-X special in this way. However, in the absence of tissue-specific deletion of this ligand at the IX-X melanoblast cluster, there is no conclusive evidence for a local source of the ligand. Stem cell factor/Kit signaling could operate in a similar way as Dct^+ melanoblasts are severely reduced in the location of nerve IX-X cluster in $Kit^{W\text{-}v}$ mutant mice at E10.5 (Mackenzie et al., 1997). We find that in Ednrb mutant mice not only is expansion of melanocyte cell number affected, but also their dispersion and migration from the nerves. A similar role has been assigned to Kit because overexpression expands and homes melanocytes (Jordan and Jackson, 2000b; Kunisada et al., 1998a; Kunisada et al., 1998b; Mackenzie et al., 1997; Steel et al., 1992; Yoshida et al., 2001).

Transcriptional cross-repression between *Sox2* and *Mitf* determines SCP and melanocyte fates

We found that glial cells in the proximal part of the nerves display the strongest expression of Sox2 with a progressive decline distally in ventral spinal nerves. Interestingly, Sox2 expression was mutually exclusive with that of Mitf. Sox2 is not believed to be essential in early NC development, but has been reported to prevent terminal differentiation of Schwann cells (Le et al., 2005; Wakamatsu et al., 2004). We find that Sox2 also plays an important role in the specification of melanocytes by maintaining a NCC fate and repressing a melanocyte fate. Sox2 was even able to abort melanocyte differentiation in cells already specified to take up such a fate, and loss of Sox2 function in mice led to increased numbers of $Mitf^+$ cells at the expense of $Sox10^+$ NCCs. Foxd3 can also repress *Mitf*, at least in vitro (Thomas and Erickson, 2009) but Sox2 appears not to regulate Mitf expression via Foxd3, as we did not observe any dependency of Foxd3 expression on Sox2 or Erbb3 (supplementary material Fig. S17). Instead, we show that Sox2 directly binds and regulates *Mitf* via the Mitf-m promoter. Combined, these results show that Sox2 has direct effects on the number of melanoblasts generated from SCPs and that downregulation of Sox2 in SCPs is a prerequisite for differentiation into melanocytes. Thus, the graded levels of Sox2 in nerves might make SCPs susceptible for an induction of Mitf and differentiation into melanocytes.

Suppression of Sox2 is also required for differentiation of immature Schwann cells into myelinating Schwann cells. Intriguingly, the Egr2 (also known as Krox20) transcription factor that is required for the transition from a promyelinating to a myelinating phenotype shows a genetic cross-regulatory suppression with Sox2 (Le et al., 2005). Hence, the results of the present study contribute to the emergence of a general logic for development of SCPs into myelinating Schwann cells and melanocytes: Sox2 maintains a SCP progenitor state and its cross-regulatory interaction with either Egr2 or Mitf consolidates myelinating Schwann or melanocyte fates, respectively (schematically illustrated in Fig. 6H).

Acknowledgements
We thank Makoto Mochii, Michael Wegner, Vince Hearing and Yoshio Wakamatsu for the generous gifts of antibodies directed against Mitf, Sox10, DCT and MEBL-1, respectively. We also thank Carlos Villaescusa for experimental support and Per Uhlen for the essential help with 3D imaging.

Funding
This work was supported by the Swedish Research Council, the Swedish foundation for strategic research and Linné grants (CEDB and DBRM grants), the Swedish Cancer Foundation and Swedish Child Cancer Foundation, the Swedish Brain Foundation, SFO-Neuroscience, Bertil Hållsten Research Foundation, EU FP7 MOLPARK collaborative project, and ERC advanced grant [232675 to P.E.]. I.A. was supported by the Swedish Research Council and Knut and Alice Wallenberg Foundation (CLICK Imaging Facility). F.L. was supported by the Swedish Medical Research Council [K2007-77PK-20285-01-6] and the European Union [Marie Curie MEIF-CT-2006-039237]. S.A. was the recipient of a Federation of European Biochemical Societies (FEBS) Long-Term Fellowship. U.S. was supported by the Swiss National Science Foundation and the National Center for Competence in Research Neural Plasticity and Repair.

Competing interests statement
The authors declare no competing financial interests.

Supplementary material
Supplementary material available online at
http://dev.biologists.org/lookup/suppl/doi:10.1242/dev.065581/-/DC1

References

Adameyko, I. and Lallemend, F. (2010). Glial versus melanocyte cell fate choice: Schwann cell precursors as a cellular origin of melanocytes. *Cell. Mol. Life Sci.* **67**, 3037-3055.
Adameyko, I. I., Mudry, R. E., Houston-Cummings, N. R., Veselov, A. P., Gregorio, C. C. and Tevosian, S. G. (2005). Expression and regulation of mouse SERDIN1, a highly conserved cardiac-specific leucine-rich repeat protein. *Dev. Dyn.* **233**, 540-552.
Adameyko, I., Lallemend, F., Aquino, J. B., Pereira, J. A., Topilko, P., Muller, T., Fritz, N., Beljajeva, A., Mochii, M., Liste, I. et al. (2009). Schwann cell precursors from nerve innervation are a cellular origin of melanocytes in skin. *Cell* **139**, 366-379.
Alizadeh, A., Fitch, K. R., Niswender, C. M., McKnight, G. S. and Barsh, G. S. (2008). Melanocyte-lineage expression of Cre recombinase using Mitf regulatory elements. *Pigment Cell Melanoma Res.* **21**, 63-69.
Andang, M., Hjerling-Leffler, J., Moliner, A., Lundgren, T. K., Castelo-Branco, G., Nanou, E., Pozas, E., Bryja, V., Halliez, S., Nishimaru, H. et al. (2008). Histone H2AX-dependent GABA(A) receptor regulation of stem cell proliferation. *Nature* **451**, 460-464.
Aquino, J. B., Hjerling-Leffler, J., Koltzenburg, M., Edlund, T., Villar, M. J. and Ernfors, P. (2006). In vitro and in vivo differentiation of boundary cap neural crest stem cells into mature Schwann cells. *Exp. Neurol.* **198**, 438-449.
Baker, C. V., Bronner-Fraser, M., Le Douarin, N. M. and Teillet, M. A. (1997). Early- and late-migrating cranial neural crest cell populations have equivalent developmental potential in vivo. *Development* **124**, 3077-3087.
Baxter, L. L. and Pavan, W. J. (2003). Pmel17 expression is Mitf-dependent and reveals cranial melanoblast migration during murine development. *Gene Expr. Patterns* **3**, 703-707.
Bernex, F., De Sepulveda, P., Kress, C., Elbaz, C., Delouis, C. and Panthier, J. J. (1996). Spatial and temporal patterns of c-kit-expressing cells in WlacZ/+ and WlacZ/WlacZ mouse embryos. *Development* **122**, 3023-3033.
Bondurand, N., Pingault, V., Goerich, D. E., Lemort, N., Sock, E., Le Caignec, C., Wegner, M. and Goossens, M. (2000). Interaction among SOX10, PAX3 and Mitf, three genes altered in Waardenburg syndrome. *Hum. Mol. Genet.* **9**, 1907-1917.
Budi, E. H., Patterson, L. B. and Parichy, D. M. (2011). Post-embryonic nerve-associated precursors to adult pigment cells: genetic requirements and dynamics of morphogenesis and differentiation. *PLoS Genet.* **7**, e1002044.
Bylund, M., Andersson, E., Novitch, B. G. and Muhr, J. (2003). Vertebrate neurogenesis is counteracted by Sox1-3 activity. *Nat. Neurosci.* **6**, 1162-1168.
Danielian, P. S., Muccino, D., Rowitch, D. H., Michael, S. K. and McMahon, A. P. (1998). Modification of gene activity in mouse embryos in utero by a tamoxifen-inducible form of Cre recombinase. *Curr. Biol.* **8**, 1323-1326.
Dorris, F. (1938). The production of pigment in vitro by chick neural crest. *Arch. Entwicklungsmech. Organ.* **138**, 323-334.
Dorris, F. (1939). The production of pigment by chick neural crest in grafts to the 3-day limb bud. *J. Exp. Zool.* **86**, 315-345.
Druckenbrod, N. R. and Epstein, M. L. (2009). Age -dependent changes in the gut environment restrict the invasion of the hindgut by enteric neural progenitors. *Development* **136**, 3195-3203.
Druckenbrod, N. R., Powers, P. A., Bartley, C. R., Walker, J. W. and Epstein, M. L. (2008). Targeting of endothelin receptor-B to the neural crest. *Genesis* **46**, 396-400.
DuShane, G. (1935). An experimental study of the origin of pigment cells in amphibian. *J. Exp. Zool.* **72**, 1-31.
Ernfors, P. (2010). Cellular origin and developmental mechanisms during the formation of skin melanocytes. *Exp. Cell Res.* **316**, 1397-1407.

Favaro, R., Valotta, M., Ferri, A. L., Latorre, E., Mariani, J., Giachino, C., Lancini, C., Tosetti, V., Ottolenghi, S., Taylor, V. et al. (2009). Hippocampal development and neural stem cell maintenance require Sox2-dependent regulation of Shh. *Nat. Neurosci.* **12**, 1248-1256.

Huber, A. B., Kania, A., Tran, T. S., Gu, C., De Marco Garcia, N., Lieberam, I., Johnson, D., Jessell, T. M., Ginty, D. D. and Kolodkin, A. L. (2005). Distinct roles for secreted semaphorin signaling in spinal motor axon guidance. *Neuron* **48**, 949-964.

Jessen, K. R. and Mirsky, R. (2002). Signals that determine Schwann cell identity. *J. Anat.* **200**, 367-376.

Jessen, K. R. and Mirsky, R. (2005). The origin and development of glial cells in peripheral nerves. *Nat. Rev. Neurosci.* **6**, 671-682.

Jin, E. J., Erickson, C. A., Takada, S. and Burrus, L. W. (2001). Wnt and BMP signaling govern lineage segregation of melanocytes in the avian embryo. *Dev. Biol.* **233**, 22-37.

Jordan, S. A. and Jackson, I. J. (2000a). A late wave of melanoblast differentiation and rostrocaudal migration revealed in patch and rump-white embryos. *Mech. Dev.* **92**, 135-143.

Jordan, S. A. and Jackson, I. J. (2000b). MGF (KIT ligand) is a chemokinetic factor for melanoblast migration into hair follicles. *Dev. Biol.* **225**, 424-436.

Kitamura, K., Takiguchi-Hayashi, K., Sezaki, M. and Yamamoto. (1992). Avian neural crest cells express a melanogenic trait migration from the neural tube: observations with the antibody, "MEBL-1". *Development* **114**, 367-378.

Krispin, S., Nitzan, E., Kassem, Y. and Kalcheim, C. (2010). Evidence for a dynamic spatiotemporal fate map and early fate restrictions of premigratory avian neural crest. *Development* **137**, 585-595.

Kunisada, T., Lu, S. Z., Yoshida, H., Nishikawa, S., Mizoguchi, M., Hayashi, S., Tyrrell, L., Williams, D. A., Wang, X. and Longley, B. J. (1998a). Murine cutaneous mastocytosis and epidermal melanocytosis induced by keratinocyte expression of transgenic stem cell factor. *J. Exp. Med.* **187**, 1565-1573.

Kunisada, T., Yoshida, H., Yamazaki, H., Miyamoto, A., Hemmi, H., Nishimura, E., Shultz, L. D., Nishikawa, S. and Hayashi, S. (1998b). Transgene expression of steel factor in the basal layer of epidermis promotes survival, proliferation, differentiation and migration of melanocyte precursors. *Development* **125**, 2915-2923.

Kushimoto, T., Basrur, V., Valencia, J., Matsunaga, J., Vieira, W. D., Ferrans, V. J., Muller, J., Appella, E. and Hearing, V. J. (2001). A model for melanosome biogenesis based on the purification and analysis of early melanosomes. *Proc. Natl. Acad. Sci. USA* **98**, 10698-10703.

Le, N., Nagarajan, R., Wang, J. Y., Araki, T., Schmidt, R. E. and Milbrandt, J. (2005). Analysis of congenital hypomyelinating Egr2Lo/Lo nerves identifies Sox2 as an inhibitor of Schwann cell differentiation and myelination. *Proc. Natl. Acad. Sci. USA* **102**, 2596-2601.

Leone, D. P., Genoud, S., Atanasoski, S., Grausenburger, R., Berger, P., Metzger, D., Macklin, W. B., Chambon, P. and Suter, U. (2003). Tamoxifen-inducible glia-specific Cre mice for somatic mutagenesis in oligodendrocytes and Schwann cells. *Mol. Cell. Neurosci.* **22**, 430-440.

Mackenzie, M. A., Jordan, S. A., Budd, P. S. and Jackson, I. J. (1997). Activation of the receptor tyrosine kinase Kit is required for the proliferation of melanoblasts in the mouse embryo. *Dev. Biol.* **192**, 99-107.

Marmigere, F. and Ernfors, P. (2007). Specification and connectivity of neuronal subtypes in the sensory lineage. *Nat. Rev. Neurosci.* **8**, 114-127.

Marmigere, F., Montelius, A., Wegner, M., Groner, Y., Reichardt, L. F. and Ernfors, P. (2006). The Runx1/AML1 transcription factor selectively regulates development and survival of TrkA nociceptive sensory neurons. *Nat. Neurosci.* **9**, 180-187.

Maro, G. S., Vermeren, M., Voiculescu, O., Melton, L., Cohen, J., Charnay, P. and Topilko, P. (2004). Neural crest boundary cap cells constitute a source of neuronal and glial cells of the PNS. *Nat. Neurosci.* **7**, 930-938.

McKeown, S. J., Lee, V. M., Bronner-Fraser, M., Newgreen, D. F. and Farlie, P. G. (2005). Sox10 overexpression induces neural crest-like cells from all dorsoventral levels of the neural tube but inhibits differentiation. *Dev. Dyn.* **233**, 430-444.

Mochii, M., Mazaki, Y., Mizuno, N., Hayashi, H. and Eguchi, G. (1998). Role of Mitf in differentiation and transdifferentiation of chicken pigmented epithelial cell. *Dev. Biol.* **193**, 47-62.

Noden, D. M. (1975). An analysis of migratory behavior of avian cephalic neural crest cells. *Dev. Biol.* **42**, 106-130.

Potterf, S. B., Furumura, M., Dunn, K. J., Arnheiter, H. and Pavan, W. J. (2000). Transcription factor hierarchy in Waardenburg syndrome: regulation of MITF expression by SOX10 and PAX3. *Hum. Genet.* **107**, 1-6.

Rawles, M. E. (1947). Origin of pigment cells from the neural crest in the mouse embryo. *Physiol. Zool.* **20**, 248-266.

Sandelin, A., Alkema, W., Engstrom, P., Wasserman, W. W. and Lenhard, B. (2004). JASPAR: an open-access database for eukaryotic transcription factor binding profiles. *Nucleic Acids Res.* **32**, D91-D94.

Srinivas, S., Watanabe, T., Lin, C. S., William, C. M., Tanabe, Y., Jessell, T. M. and Costantini, F. (2001). Cre reporter strains produced by targeted insertion of EYFP and ECFP into the ROSA26 locus. *BMC Dev. Biol.* **1**, 4.

Steel, K. P., Davidson, D. R. and Jackson, I. J. (1992). TRP-2/DT, a new early melanoblast marker, shows that steel growth factor (c-kit ligand) is a survival factor. *Development* **115**, 1111-1119.

Steingrimsson, E., Copeland, N. G. and Jenkins, N. A. (2004). Melanocytes and the microphthalmia transcription factor network. *Annu. Rev. Genet.* **38**, 365-411.

Thomas, A. J. and Erickson, C. A. (2009). FOXD3 regulates the lineage switch between neural crest-derived glial cells and pigment cells by repressing MITF through a non-canonical mechanism. *Development* **136**, 1849-1858.

Twitty, V. (1936). Correlated genetic and embryological experiments on triturus. *J. Exp. Zool.* **74**, 239-302.

Wakamatsu, Y., Maynard, T. M. and Weston, J. A. (2000). Fate determination of neural crest cells by NOTCH-mediated lateral inhibition and asymmetrical cell division during gangliogenesis. *Development* **127**, 2811-2821.

Wakamatsu, Y., Endo, Y., Osumi, N. and Weston, J. A. (2004). Multiple roles of Sox2, an HMG-box transcription factor in avian neural crest development. *Dev. Dyn.* **229**, 74-86.

Watanabe, A., Takeda, K., Ploplis, B. and Tachibana, M. (1998). Epistatic relationship between Waardenburg syndrome genes MITF and PAX3. *Nat. Genet.* **18**, 283-286.

Watanabe, T., Saito, D., Tanabe, K., Suetsugu, R., Nakaya, Y., Nakagawa, S. and Takahashi, Y. (2007). Tet-on inducible system combined with in ovo electroporation dissects multiple roles of genes in somitogenesis of chicken embryos. *Dev. Biol.* **305**, 625-636.

Wilkie, A. L., Jordan, S. A. and Jackson, I. J. (2002). Neural crest progenitors of the melanocyte lineage: coat colour patterns revisited. *Development* **129**, 3349-3357.

Wilson, Y. M., Richards, K. L., Ford-Perriss, M. L., Panthier, J. J. and Murphy, M. (2004). Neural crest cell lineage segregation in the mouse neural tube. *Development* **131**, 6153-6162.

Woodhoo, A., Dean, C. H., Droggiti, A., Mirsky, R. and Jessen, K. R. (2004). The trunk neural crest and its early glial derivatives: a study of survival responses, developmental schedules and autocrine mechanisms. *Mol. Cell. Neurosci.* **25**, 30-41.

Yamaguchi, T. P., Bradley, A., McMahon, A. P. and Jones, S. (1999). A Wnt5a pathway underlies outgrowth of multiple structures in the vertebrate embryo. *Development* **126**, 1211-1223.

Yoshida, H., Kunisada, T., Grimm, T., Nishimura, E. K., Nishioka, E. and Nishikawa, S. I. (2001). Review: melanocyte migration and survival controlled by SCF/c-kit expression. *J. Investig. Dermatol. Symp. Proc.* **6**, 1-5.